Crosswell Seismic and Electromagnetic Monitoring of CO_2 Sequestration

G. Michael Hoversten[1], Roland Gritto[1], Thomas M. Daley[1], Ernest L. Majer[1] and Larry R. Myer[1]

Lawrence Berkeley National Laboratory

ABSTRACT

The quantitative estimation of changes in water saturation (S_w) and effective pressure (P), in terms of changes in compressional and shear impedance, is becoming routine in the interpretations of time-lapse surface seismic data. However, when the number of reservoir constituents increases to include *in situ* gas and injected CO_2, there are too many parameters to be determined from seismic velocities or impedances alone. In such situations, the incorporation of electromagnetic (EM) images showing the change in electrical conductivity (σ) provides essential independent information. The purpose of this study was to demonstrate a methodology for jointly interpreting crosswell seismic and EM data, in conjunction with detailed constitutive relations between geophysical and reservoir parameters, to quantitatively predict changes in P, S_w, CO_2 gas saturation (S_{CO2}), CO_2 gas/oil ratio (R_{CO2}), hydrocarbon gas saturation (S_g), and hydrocarbon gas/oil ration (R_g) in a reservoir undergoing CO_2 flood.

INTRODUCTION

Crosswell seismic and EM technology has been developed over the past two decades to provide high spatial resolution images of the compressional velocity (V_p), shear velocity (V_s) and the σ of the inter-well region. Much of the effort, as measured by the topics of published and presented work, has concentrated on developing and improving algorithms for estimating the geophysical parameters themselves. In most reported applications, the output from a survey is a cross section of V_p, V_s, or σ, or the time-lapse change (Δ) of these parameters, which is discussed in terms of its implications for the distribution and/or Δ of the reservoir parameter of interest. These interpretations are qualitative and can be in error when more than one reservoir parameter affects the geophysical parameter.

In many settings, the geophysical parameters depend on a number of reservoir parameters that are variable in both space and time. In particular ϕ, P, S_w, and S_g strongly influence V_p. σ can generally be described as a function of ϕ, S_w and fluid σ [1]. As we will show in a multicomponent fluid reservoir, the spatial distribution of the time-lapse change in geophysical parameters, such as V_p, can differ significantly from the spatial distribution of the time-lapse change in a desired reservoir parameter such as R_{CO2}. This difference results from the geophysical parameters dependence on other parameters such as P and S_w, which must be sorted out before a picture of any single reservoir parameter can be obtained.

The objective of the work described in this paper is to demonstrate a methodology for combining time-lapse changes in σ, V_p, and V_s with a detailed rock-properties model to produce quantitative estimates of the change in R_{CO2} and $S_{CO2.}$

EXPERIMENT DESCRIPTION

Crosswell seismic and EM measurements were conducted in the Lost Hills oil field in southern California during a CO_2 injection pilot study conducted by Chevron Petroleum Co. The P and temperature (T) of the reservoir make this an immiscible flood; CO_2 is in the gas phase within the reservoir. The experiment took place in a portion of the field that had been undergoing water flood since 1995. Two observation wells, OB-C1 and OB-C2, were drilled for the pilot and fiberglass cased to allow the use of crosswell EM. The nearby CO_2 injector (11-8WR) is located just 6 m (20 feet) out of the crosswell-imaging plane. The injection wells are hydraulically fractured to increase injectivity into the low permeability diatomite reservoir. In some cases, downhole pressures were increased above the lithostatic pressure, which may have induced fracturing above the desired injection interval. If the fracture did indeed extend above the desired interval there is a high probability that much of the injected CO_2 will not sweep its intended target, but will move in the higher section.

The baseline crosswell seismic and EM surveys were conducted in September 2000, just prior to the beginning of CO_2 injection. Two seismic sources were used; a piezoelectric V_p source and an orbital vibrator V_s source with maximum frequency contents of 2000 and 350 Hz respectively. A repeat seismic survey was conducted in late May 2001, with the repeat EM survey conducted in early July 2001.

ROCK PROPERTIES MODEL

The reservoir parameters that have a dominant affect on the geophysical parameters are ϕ, P, S_w, S_g, Rg and R_{CO2}. Effective pressure, P, is equal to lithostatic minus pore pressure (P_{pore}). So as P_{pore} increases, P will decrease. Pressure has a significant effect in Lost Hills since this is a shallow reservoir in soft rock. We sought constitutive relations between geophysical and reservoir parameters (rock-properties model) that would be able to predict observed V_p, density and σ from observed P, ϕ, S_w, and S_g. Laboratory measurements of the dry frame moduli and grain density of the diatomite reservoir rock were unavailable, so Hertz-Mindlin theory with the modified Hashin-Strikman [2] lower bound was used to model the dry-frame moduli of the reservoir rock. Fluid substitution in the dry frame is modeled by Gassmann's equation. The bulk moduli and densities of gas, live oil and brine, as well as R_g, are modeled using relations published by Betzel and Wang [3]. The bulk σ of the reservoir rock is modeled using Archie's [1] relationship.

A simplex algorithm was used to solve for the model parameters that would minimize the combined miss-fit between observed V_p and density logs and the model predictions given the ϕ, S_w and S_g logs. The results of this minimization, along with the Archie's law fit to the OBC1 σ log, are shown in Figure 1(a) - (d).

The pressure-prediction capability of the model was validated by comparison to laboratory measurements on core samples of diatomite from the Lost Hills field. Figure 1(e) presents the measured data recast as ΔV_p as a function of ΔP at a reference P of 4.7 MPa, the effective pressure in the reservoir at the start of CO_2 injection. The model predictions are within a few percent of the lab measurements for vertical V_p over the expected range of pressure decrease, from 0 to 2.5 MPa from the initial pressure.

The rock-properties model is used to calculate changes in V_p, V_s, and σ as functions of changes in P, S_w, S_g, and S_{CO2} when certain reference values of P, ϕ, S_w, and S_g are assumed. Figure 2 shows ΔV_p and ΔV_s as functions of ΔP and ΔS_w about a reference point (reservoir just prior to CO_2 injection) where S_w, ϕ, and P are equal to 0.5, 0.5, and 4.7 (MPa) respectively. Relations between ΔV_p and ΔV_s and ΔP and ΔS_w, such as illustrated in Figure 2(a) and (c), form the basis of 4D seismic ΔP and ΔS_w prediction. However, when S_g is non-zero, as shown in Figure 2(b), the orientation and magnitude of contours of constant ΔV_p change dramatically. The change in V_s is only slightly effected (through density) by the presence of gas. Without additional information, ΔV_p and ΔV_s are insufficient to predict ΔP, ΔS_w and ΔS_g. EM data provides an independent estimate of ΔS_w. Electrical conductivity (σ) is a much simpler function of reservoir parameters than is the velocity and can be described by Archie's law [1]. Assuming ϕ is constant, $\Delta\sigma$ is only a function of ΔS_w and Δ pore σ. Since water flood has been in effect for over 6 years, we assume that the pore-fluid water has reached equilibrium between injected and native water, and fluid σ does not change. Therefore, conductivity changes are interpreted solely in terms of water saturation changes.

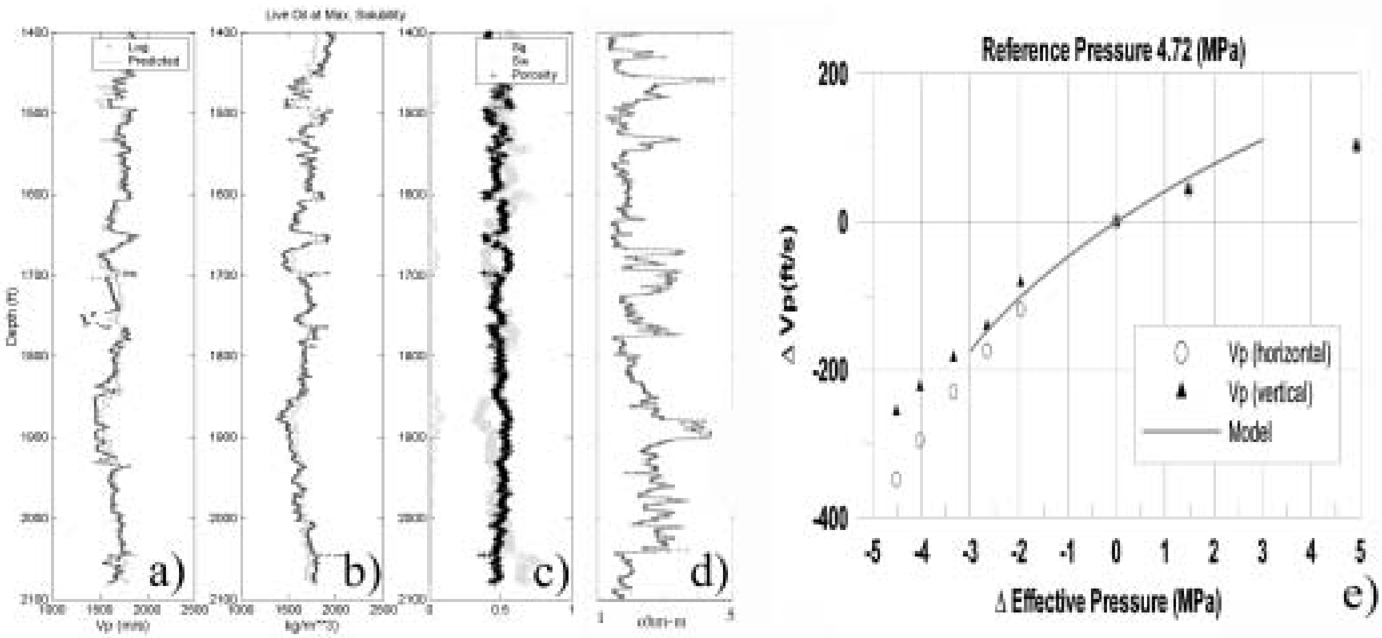

Figure 1: Rock-properties model uses logged porosity (+), water saturation (box) and gas saturation (dots) shown in (c) as inputs in a multi-parameter simplex regression to predict the V_p (a), density (b) and electrical resistivity (d). Measured V_p, density and resistivity are shown as dots, model predicted values are shown as lines. Panel (e) is ΔVp as a function of ΔP (solid curve) compared to measured vertical (triangles) and horizontal (circle) ΔVp from laboratory measurements.

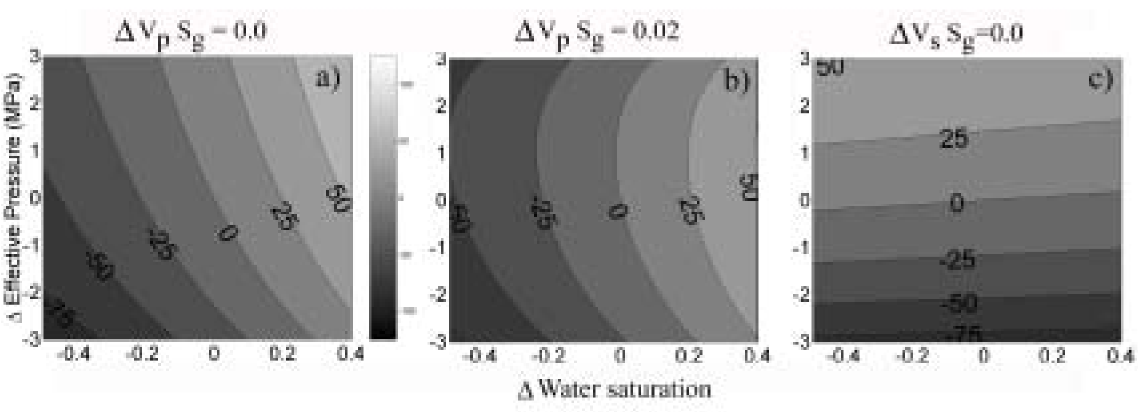

Figure 2: Changes in P and S wave velocity (m/s) as functions of changes in effective pressure and water saturation. Panel (**a**) ΔV_p with S_g = 0.0, panel (**b**) ΔV_p with S_g = 0.02, panel (**c**) ΔV_s with S_g = 0.0. ΔVs is essentially independent of S_g. All calculations are done at a reference S_w, ϕ and P of 0.5, 0.5 and 4.7 MPa.

INTEGRATED TIME-LAPSE GEOPHYSICAL IMAGES

The strategy we adopted to maximize the spatial correlation between V_p, V_s, and σ images was to begin with the EM where the most *a priori* information existed, then use the σ images to produce starting V_p models, and then follow that by producing starting V_s models from the final V_p models. We chose to use a conjugate gradient algorithm [5] because the final model is sensitive to the initial model and is perturbed from the starting values only as much as needed to fit the observed data.

The EM inversion [4] for the data at initial conditions was started from a model built by laterally interpolating the σ logs between the OB-C1 and OB-C2 wells. The EM inverse σ model at initial conditions was then used as the starting model for the inversion of the July 2001 EM data. Differencing these inversions provides the $\Delta\sigma$ shown in Figure 3©. There is a high degree of correlation between the 11-8WR permeability log and the areas where the largest decrease in σ occur. The correlation between high permeability and large changes in S_w, and thus σ, is expected. Also, the largest σ changes occur more in alignment with the estimated location of the old water injection fracture than with the much newer CO_2 fracture. This is not surprising when we consider that the water injection was ongoing for more that 6 years and thus likely produced a high permeability damage zone that is a better conduit for flow than the very new CO_2 fracture.

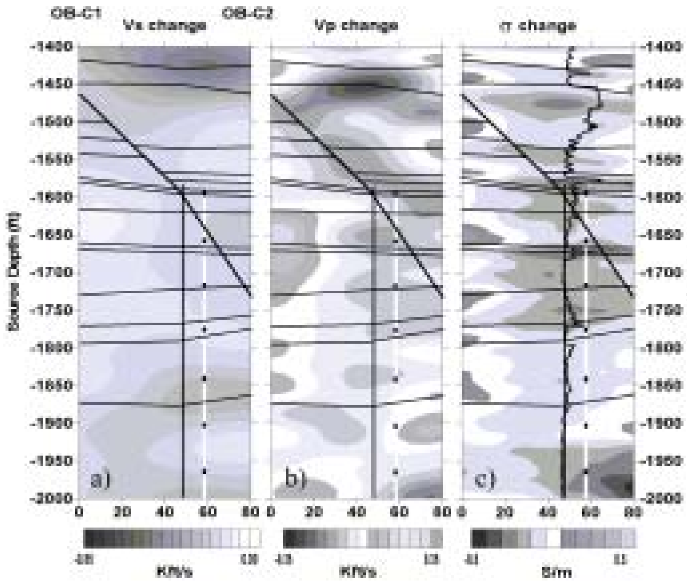

Figure 3: Time-lapse changes in (a) V_s, (b) V_p and (c) σ. Major unit boundaries are shown as black horizontal lines, estimated location of previous water injection fracture is vertical line (x=45 ft), estimated location of the CO_2 injection fracture is shown as a vertical white line (x=6 0ft), perforation intervals for CO_2 injection are shown as black dots, location of a fault zone is shown as the black diagonal line. The permeability log from the CO_2 injection well 11-8WR is shown in black on panel (c).

Next, the pre- and post-CO_2 σ models were converted to V_p. These were then used as initial models in the inversion of the V_p travel time data to produce the change in V_p shown in Figure 3(b). In addition to V_p changes occurring in the vicinity of the estimated water-injection fracture, there are decreases in V_p that align with the mapped fault. Since there is no σ changes obviously correlated with the fault, we interpret this to mean that pressure changes are occurring along the fault zone advanced in time relative to significant changes in water saturation.

The V_p sections were converted to V_s using a V_p/V_s ratio derived from the rock properties model and used as starting models for the V_s travel time inversions resulting in the ΔV_s section shown in Figure 3(a). The ΔV_s section is smoother than either the $\Delta\sigma$ or ΔV_p sections, due in part to the lower frequency content in the shear wave data. The ΔV_s section is also smoother because Vs is relatively insensitive to ΔS_w, which has high spatial variability, but very sensitive to ΔP, that has much lower spatial variability. Even with the smoother spatial changes in the V_s data, we see correlation with the V_p and σ changes. In particular, the zone along the fault shows a decrease in V_s, lending support to our interpretation that pressure is changing along the fault zone.

PREDICTING CHANGES IN RESERVOIR PARAMETERS

First the $\Delta\sigma$ image was used to predict ΔS_w, assuming that ϕ and fluid σ did not change. The predicted ΔS_w was used with the observed ΔV_s and the relation illustrated in Figure 2(c) to predict ΔP. The predicted ΔS_w and ΔP were then used to calculate the ΔV_p that would be caused by ΔS_w and ΔP alone, assuming S_g=0. Over the majority of the image plane, ΔS_w and ΔP are negative thus producing a negative ΔV_p. The difference between the observed and calculated ΔV_p (ΔV_R) was generated. We expect the CO_2 to decrease V_p in excess of the effects of ΔS_w and ΔP alone. There are two mechanisms for CO_2 to decrease V_p: 1) through decreasing the bulk modulus of the oil by increasing R_{CO2} and 2) by increasing S_{CO2} through introduction of free CO_2. Either of these mechanisms would produce a negative ΔV_R. On the other hand, a $+\Delta V_R$ can result if the assumption S_g=0, is incorrect. The presence of initial gas will produce this effect, as seen by comparing Figure 2(a) and 2(b) where the presence of gas reduces the decrease in V_p associated with a given ΔS_w and ΔP. If *in situ* hydrocarbon gas is present and has been accounted for in the calculation of ΔV_R, $+\Delta V_R$ can result when S_g is reduced, as the pore pressure increase dissolves gas into the oil.

The OB-C1 log showed the presence of hydrocarbon gas over certain intervals within the reservoir. Therefore a two-step process was used to calculate ΔV_R. The first pass used S_g=0 as described. Next, sections of the image with $+\Delta V_R$ were recalculated assuming S_g = 0.02 (the average non-zero S_g in the reservoir interval). After the second pass calculation of ΔV_R, much of the areas that had $+\Delta V_R$ after the first pass became negative. The final ΔV_R was converted to ΔR_{CO2} by a linear interpolation, since ΔV_R is a linear function of ΔR_{CO2}.

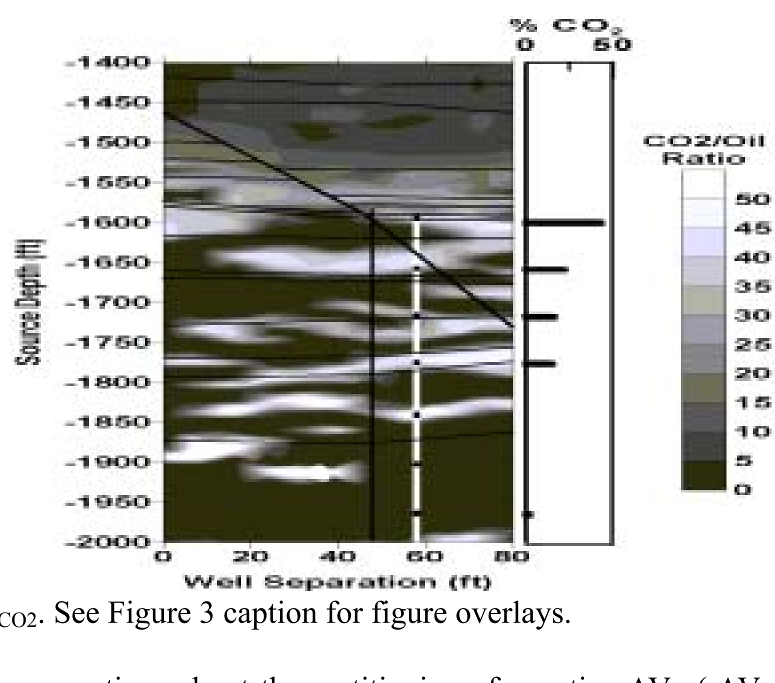

Figure 4: Predicted ΔR_{CO2}. See Figure 3 caption for figure overlays.

This final step requires assumptions about the partitioning of negative ΔV_R ($-\Delta V_R$). First we assumed that the $+\Delta P_{pore}$ caused by injection would drive as much of the initial hydrocarbon S_g into the oil as possible. Next, we assume a partitioning between the $+\Delta R_{CO2}$ and $+\Delta S_{CO2}$ effects on ΔV_R. We chose to allow the maximum increase in R_{CO2} for the given $+\Delta P_{pore}$ and ΔS_w. Areas of $-\Delta V_R$ were converted to $+\Delta R_{CO2}$ up to the maximum R_{CO2} for the final P_{pore} and T. The observed $-\Delta V_R$ could be completely accounted for by $+\Delta R_{CO2}$ without requiring $+\Delta S_{CO2}$. Figure 4 shows the calculated ΔR_{CO2} generated from the geophysical parameter changes shown in Figure 3. As has been stated, these calculations are based on differences calculated at reference values of P, ϕ, S_w and S_g. The sensitivity of the ΔR_g and ΔS_g predictions to the reference parameters has been studied. These studies show that the calculations are relatively insensitive to the reference ϕ and S_w values. The calculations are most sensitive to the assumed hydrocarbon gas saturation, with incorrect assignment of S_g producing errors in predicted ΔR_{CO2} of 10 - 15 %. The next largest source of error is the choice of the reference P, with a 15% error in the reference P producing errors in ΔR_{CO2} of approximately 10%.

The predicted ΔR_{CO2} (Figure 4) shows a strong correlation with the location of perforation intervals that account for the majority of the injected CO_2. The percentage of injected CO_2 going into each perforation is plotted to the right of Figure 4 and shows that the upper four perforations account for 95% of all the CO_2. Almost 50% of the CO_2 goes into the upper most perforation. The location of this perforation corresponds with the large $+\Delta R_{CO2}$ associated with the fault zone and region above, indicating loss of substantial CO_2 into the upper portions of the reservoir. The next three perforations down account for roughly another 45% of CO_2 injected with each perforation aligning with a laminar zone of $+\Delta R_{CO2}$. The only poor correlation between injected CO_2 and predicted $+\Delta R_{CO2}$ occurs at the perforation at a depth of 564 m (1850 ft). At this depth a laminar $+\Delta R_{CO2}$ zone aligns with a perforation, but the injectivity log indicates little injected CO_2.

CONCLUSION

We have demonstrated that by combining seismically derived ΔV_p and ΔV_s with EM derived $\Delta\sigma$, estimates of ΔP, ΔS_w and ΔR_{CO2} can be made in a complex reservoir containing oil, water, hydrocarbon gas, and introduced CO_2. The resulting predicted ΔR_g is better correlated with measured CO_2 injectivity than are any of the time-lapse geophysical parameter images. The predicted ΔR_g images indicate that a significant portion of the injected CO_2 is filling the upper portions of the section above the intended injection interval. These conclusions are validated by CO_2 injectivity measurements made in the 11-8WR well.

The methodology outlined in this paper relies on many assumptions that were required because the project was not designed to use this methodology. However, in future applications these assumptions could be substantially reduced by design. In particular, considerable benefit could be drawn from repeat logging of the wells with a full suite of logs. This would provide control points for the ΔP, ΔS_w, ΔS_g, ΔV_p, ΔV_s, and $\Delta\sigma$, all of which would serve to greatly constrain the problem. In addition, having full log suites would enable much better control of the geophysical inverse solutions through superior starting models.

Acknowledgements

Support was provided by the Assistant Secretary for Fossil Energy, Office of Coal and Power Systems through the National Energy Technology Laboratory of the US Department of Energy under Contract No. DE-AC03-76SF00098.

References

1. Archie, G.E., (1942). The Electrical Resistivity Log as an Aid in Determining Some Reservoir Characteristics. *Trans. Am. Inst. Mech. Eng.* 146, 54 - 62.
2. Hashin, Z. and Shtrikman, S. (1963). A Variational Approach to the Elastic Behavior of Multiphase Materials, *J. Mech. Phys. Solids* **11**, 127 – 140.
3. Betzel, M. and Wang, Z. (1992). Seismic Properties of Pore Fluids, *Geophys*. **57**, 1396 - 1408.
4. Newman, G.A. (1995), Crosswell Electromagnetic Inversion Using Integral and Differential Equations. *Geophysics*, **60**, 899 - 911.
5. Jackson, M.J. and Tweeton, D.R. (1996), *3DTOM: Three-Dimensional Geophysical Tomography*, U.S. Department of the Interior, Bureau of Mines, Report of Investigation 9617.